CrossMark

RESEARCH ARTICLE

Monsoon-driven transport of atmospheric mercury to the South China Sea from the Chinese mainland and Southeast Asia—Observation of gaseous elemental mercury at a background station in South China

Ming Liu[1] · Laiguo Chen[1] · Donghai Xie[2] · Jiaren Sun[1] · Qiusheng He[3] · Limei Cai[4] ·
Zhiqiang Gao[1] · Yiqiang Zhang[1]

Abstract Concentrations of gaseous elemental mercury (GEM) were continuously monitored from May 2011 to May 2012 at the Wuzhishan State Atmosphere Background Monitoring Station (109°29′30.2″ E, 18°50′11.0″ N) located in Hainan Island. This station is an ideal site for monitoring long-range transport of atmospheric pollutants from mainland China and Southeast Asia to South China Sea. Annual average GEM concentration was 1.58 ± 0.71 ng m^{-3} during the monitoring period, which was close to background values in the Northern Hemisphere. GEM concentrations showed a clear seasonal variation with relatively higher levels in autumn (1.86 ± 0.55 ng m^{-3}) and winter (1.80 ± 0.62 ng m^{-3}) and lower levels in spring (1.16 ± 0.45 ng m^{-3}) and summer (1.43 ± 0.46 ng m^{-3}). Long-range atmospheric transport dominated by monsoons was a dominant factor influencing the seasonal variations of GEM. The GEM diel trends were related to the wind speed and long-range atmospheric mercury transport. We observed 30 pollution episodes throughout the monitoring period. The analysis of wind direction and backward trajectory suggested that elevated GEM concentrations at the monitoring site were primarily related to the outflows of atmospheric Hg from mainland China and the Indochina peninsula. The △GEM/△CO values also suggested that GEM was significantly affected by the long-range transport from the anthropogenic sources and biomass burning in Asia and Indochina peninsula.

Keywords Gaseous elemental mercury (GEM) · Seasonal monsoons · Long-range transport · Back trajectories · GEM/CO ratio

✉ Laiguo Chen
  631811743@qq.com; chenlaiguo@scies.org

✉ Donghai Xie
  105411639@qq.com

1   Urban Environment and Ecology Research Center, the Key Laboratory of Water and Air Pollution Control of Guangdong Province, South China Institute of Environmental Sciences (SCIES), Ministry of Environmental Protection (MEP), Guangzhou 510655, China

2   Hainan Research Academy of Environmental Sciences, Haikou 571126, China

3   School of Environment and Safety, Taiyuan University of Science and Technology, Taiyuan 030024, China

4   Ministry of Education Key Laboratory of Oil and Gas Resources and Exploration Technologies, Yangtze University, Wuhan 430100, China

Introduction

The global cycle of mercury (Hg) has attracted extensive attention from the international community. By October 2014, 128 nations formally have signed the "Minamata Convention on Mercury", which restricted the production, utilization, and emission of Hg. China is one of the signatories to this convention and has been facing great pressure because of its high emissions (UNEP/AMAP 2013; Muntean et al. 2014). China is the largest contributor to global atmospheric Hg. Total anthropogenic Hg emissions were estimated to have increased continuously from 356 t in 2000 to 538 t in 2010, representing an average annual rate of increase of 4.2 % (Zhang et al., 2015). Hg transport from mainland China has attracted global attention. Several observational and baseline studies have been performed in China, which, across the different regions in China, show variations in background location and typical

🖄 Springer

dispersion in the cities. These studies have included Waliguan and Lanzhou in Northwest China (Su et al., 2007; Fu et al., 2012a); Gongga Mountain, Leigong Mountain, and Guiyang in Southwest China (Feng et al., 2004; Fu et al., 2008, 2010a); Chongming Island, Nanjing, and Shanghai in East China (Friedli et al., 2011; Zhu et al., 2012; Dou et al., 2013); and Changbai Mountain and Changchun in Northeast China (Fang et al., 2004; Fu et al., 2012b). Generalizing these studies indicated that the seasonal variations of Hg differed in the various regions of China. In the north and southwest, coal combustion was identified as the cause of the variations in Hg (Fang et al., 2004; Feng et al., 2004). In the city of Nanjing in East China, the high average monthly concentrations were attributed to the re-volatilization of Hg deposited during the warm season due to the high temperatures and greater solar radiation (Zhu et al., 2012). In the Pearl River Delta of South China, the seasonal monsoon was identified as the reason for Hg emissions transport (Chen et al., 2013). With regard to the studies conducted for the background locations, the main factors affecting Hg levels were concluded to have been the seasonal monsoon, as well as the transport of local and regional emissions (Fu et al. 2008, 2012a). While many previous studies have measured atmospheric Hg in mainland China (Fu et al., 2008, 2009, 2010a; Chen et al. 2013), studies regarding the outflow of Hg from mainland China are limited.

China has a marked continental and oceanic monsoonal climate. The air stream flows from the ocean to the land in the summer, and this horizontal air flow reverses in the winter. In the winter, it is clear that the monsoon may transport Hg to the south and west of the Chinese mainland. Tseng et al. (2012) identified the northwest monsoon as the reason for the increased autumn and winter concentration of atmospheric Hg in the northern region of the South China Sea (SCS). The increased atmospheric Hg levels in Taiwan and Korea were attributed to long-distance monsoonal transport from the Chinese mainland (Kim et al., 2009; Sheu et al., 2010).

Hainan Island lies at the southern tip of China and is separated from the Chinese mainland by the Qiongzhou Strait, with the Beibu Gulf in the west and the South China Sea in the southeast. Hainan Island has good air quality (MEP 2014) with a very limited number of industrial emission sources because tourism is its dominant industry. This region is distinctly affected by seasonal monsoons and is, therefore, an ideal place to monitor the background level of GEM and study regional atmospheric transport. The Hg observational data in Hainan Island will be good supplements to Global Mercury Observation System (GMOS), and very valuable for further understanding of the global Hg cycle.

The aims of this study were to (1) determine the background level and variability of Hg on Hainan Island, (2) study the effect of the monsoon on the long-range transport of Hg in the South China region, and (3) understand the outflow of Hg from mainland China and Southeast Asia.

Experimental methods

Sampling site

The monitoring site for this study is located at the Wuzhishan State Atmosphere Background Monitoring Station (109°29′ 30.2″ E, 18°50′11.0″ N) at Wuzhi Mountain of Hainan Island, 958 m a.s.l. Wuzhi Mountain is located in the south-central hinterland of Hainan Island and is the highest peak in this region. This site has both mountainous and insular climate characteristics. Northeast winds and southwest winds are prevalent in the winter and the summer, respectively. The rainy season is from May to October, and the dry season is from November to April (of the next year). The average annual temperature is 22.4 °C, and the average monthly temperature is 17 °C in January and 26 °C in July. The average annual rainfall is 1690 mm, the average relative humidity is 84 %, and the average annual sunshine is approximately 2000 h. This site is ideal for monitoring the background regional atmospheric characteristics and long-range transport because of its low population density, excellent ecological environment, few anthropogenic emission sources, and long distance from the town.

Measuring time and method

The experiment was conducted from May 2011 to May 2012 using an automatic Hg vapor analyzer (model 2537B, Tekran, Toronto, Canada) in situ. The instrument has two parallel gold cartridges. While one cartridge adsorbs Hg during the sampling period, the other simultaneously analyzes the collected Hg, allowing for the continuous sampling of the ambient air. The ambient air was introduced to the inlet of the analyzer through a heated Teflon tube (45 °C) to remove the moisture. The particulate matter was removed using 45-mm-diameter PTFE filters (Whatman, 0.2 μm) installed at the inlets of the sampling Teflon tube and the analyzer. These filters were replaced every 7 to 20 days, depending on the filter load. The analyzer was programmed to measure the atmospheric Hg every 10 min with a volumetric sampling flow rate of 1.0 L min^{-1}. Speciated atmospheric Hg is operationally defined as gaseous elemental Hg (GEM), gaseous oxidized Hg (GOM), and particulate bound Hg (PBM). There has been much discussion among Hg researchers as to whether the Tekran 2537 measures total gaseous Hg (TGM, TGM = GEM + GOM), as opposed to GEM. The particle filtration device and the heated line may cause GOM losses to the filter and the tubing wall (Gustin et al., 2015). Consequently, the values obtained from our mercury measurements are considered to be close to GEM concentrations in this study. Conventional meteorological data (i.e., wind speed, wind direction, temperature, relative humidity, and pressure) were synchronously collected using a meteorological

instrument (model ZZ11B, Shanghai meteorological instrument factory, China). CO and O_3 data were measured using automatic instruments (model 49i, Thermo, USA, and model 48i, Thermo, USA, respectively).

The Tekran 2537B analyzer was automatically calibrated every 25 h using the instrument's internal mercury permeation source. These automated calibrations were tested, before and after the sampling campaign, with manual injections using a saturated mercury vapor standard from an external mercury vapor source (Tekran 2505). The relative percentage difference between the manual injections and automated calibrations was less than 10 %. The GEM detection limit in this operation mode is less than 0.1 ng m^{-3}. All concentrations are stated at the standard conditions of $P = 760$ mmHg and $T = 0$ °C.

Back trajectory analysis

The Hybrid Single-Particle Lagrangian Integrated Trajectory (HYSLPIT4.0) model and Gridded Meteorological Data (GDAS one-degree archive), which were provided by the National Oceanic and Atmospheric Administration (NOAA), were used to calculate the trajectories. The top of the model domain was set to 8000 m a.g.l. Trajectories that extended for 3 days (72 h) into the past were calculated daily at 1-hour intervals. All trajectories were analyzed statistically using TrajStat software (Wang et al. 2009). Because the values were obtained from NOAA's NCEP meteorological models, the data used for the transport and dispersion calculations are interpolated to grids of coarser resolution. The uncertainties depend upon local effects, as well as the larger scale gradients of the variable, and the degree to which a gridded field can represent a continuous function.

Determination of concentration-weighted trajectory (CWT)

The CWT for GEM for a particular concentration-weighted trajectory (CWT) grid cell (i, j) is a measure of the source strength of a grid cell and is assigned a weighted concentration, by averaging the sample concentrations of the trajectories that crossed that grid cell, as follows (Hsu et al. 2003; Kabashnikov et al. 2011):

$$\text{CWT}_{ij} = \frac{\sum_{l=1}^{M} C_l \cdot \tau_{ijl}}{\sum_{l=1}^{M} \tau_{ijl}}.$$

C_l is the 1 h GEM concentration corresponding to the arrival of the back trajectory l, l is the index of the trajectory, τ_{ijl} is the time spent in the grid cell (i, j) by the trajectory l, and M is the total number of back trajectories over a given time period (e.g., each season).

In this study, the research region is a geographical domain from 10 to 30°N and from 110 to 130°E. The geographical

domain was divided into 40,000 grid cells (200 grid cells across the latitude by 200 grid cells across the longitude) with each covering area of 0.1° by 0.1°.

Statistical analysis

Because of the normal distribution of the data (Kolmogorov-Smirnov test, $p > 0.05$), all data were statistically analyzed using the independent-sample t test and SPSS 17.0 for Windows (SPSS, Chicago, USA). The statistical test results were considered to be statistically significant at $p < 0.05$. The figures were generated using Origin 8.0 and ArcGIS 9.3.

Results and discussion

Annual GEM level at the monitoring site

During the monitoring period, the annual average GEM concentration was 1.58 ± 0.71 ng m^{-3}. This value is similar to the background values reported for the Northern Hemisphere (1.5–1.7 ng m^{-3}) (Slemr et al. 2003; Kim et al. 2005), relatively higher than those of the Southern Hemisphere (0.58–1.05 ng m^{-3}) (Slemr et al. 2015), and significantly lower than the values reported at some other background sites in mainland China, such as Waliguan (Fu et al., 2012a), Gongga Mountain (Fu et al., 2008, 2009), and Leigong Mountain (Fu et al., 2010a).

Seasonal variation of GEM and the seasonal monsoon's effect

In this study, relatively higher levels of GEM were observed in the autumn (1.86 ± 0.55 ng m^{-3}) and the winter (1.80 ± 0.62 ng m^{-3}), and relatively lower GEM concentrations were observed in the spring (1.16 ± 0.45 ng m^{-3}) and the summer (1.43 ± 0.46 ng m^{-3}) (Fig. 1). We also observed clear day-to-day variations of GEM in some months (for example,
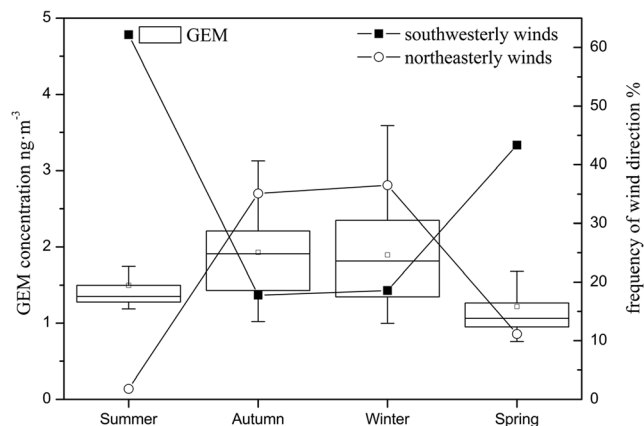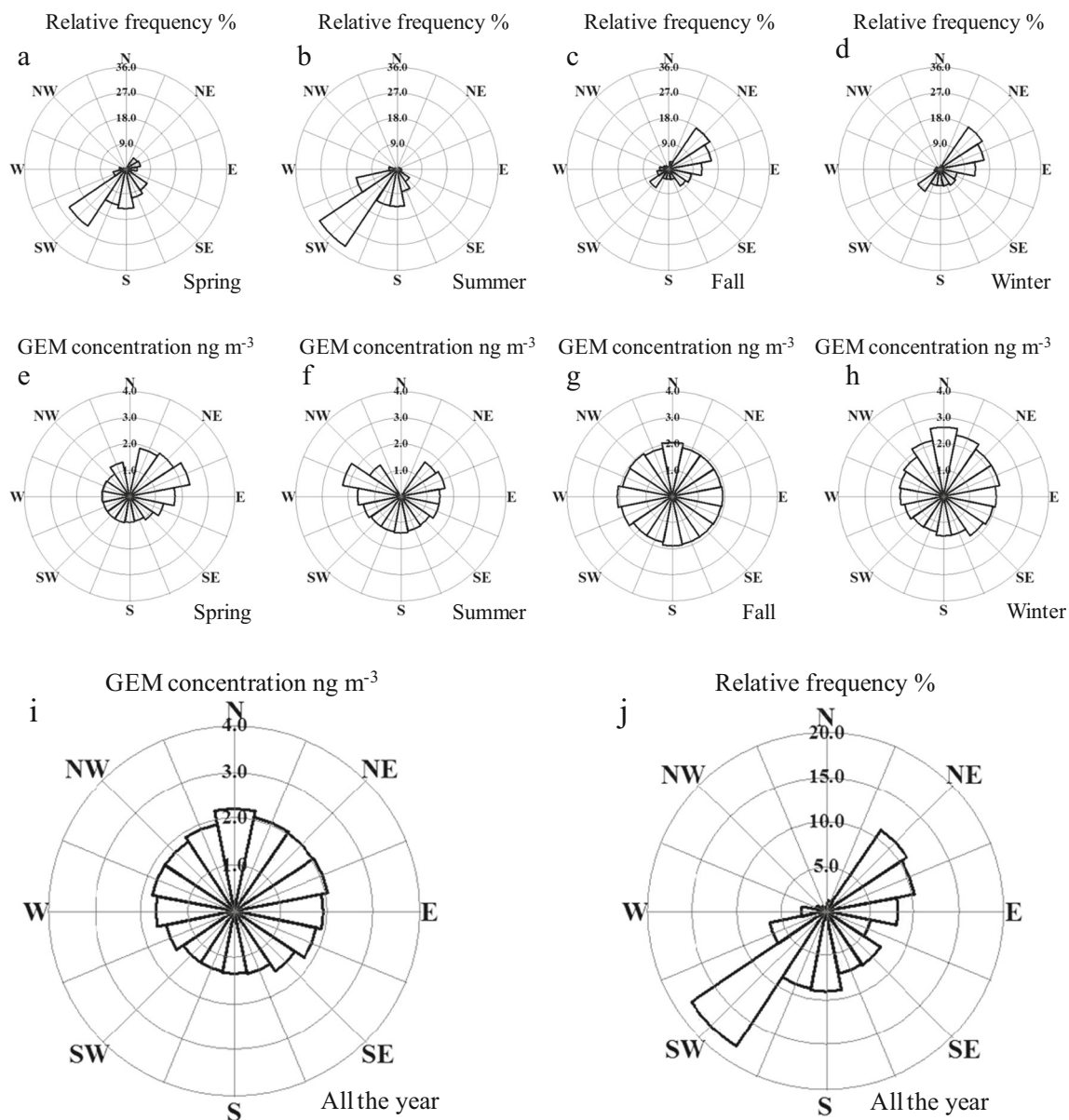

Fig. 1 Seasonal variation of GEM concentration at Wuzhi Mountain

May and September 2011), which suggest that the GEM levels at the sampling site were significantly affected by external atmospheric transport.

The wind dependence of the GEM concentrations during the monitoring period was such that the higher GEM concentrations were mostly related to the wind from the northwest, north and northeast (Fig. 2i), while the lower GEM values were observed in the prevailing southwest wind that originated from the SCS and the Western Pacific Ocean (Fu et al., 2010b). These values can be considered as the background levels.

The annual wind rose shows the prevailing winds were from the southwest and the northeast (Fig. 2j). The southwest winds prevailed in spring (March–May) and summer (June–August), with the air mass originating from the Indian Ocean

with presumably low Hg emissions levels (Fig. 2a–f). The northeast wind prevailed in autumn (September–November) and winter (December–February), with high levels (Fig. 2c–h). In the studies on urban and regional atmospheric Hg in South China and the SCS, the seasonal monsoon has been considered to have an important impact on the seasonal variations of GEM and atmospheric long-range transport (Tseng et al., 2012; Chen et al., 2013; Sheu et al., 2013). The behavior exhibited by the wind direction across all four seasons is consistent with the typical seasonal monsoon climate in this region. These results imply that the seasonal variations in GEM were significantly influenced by the seasonal monsoons. Nevertheless, these variations might also be related to the stronger atmospheric photochemical processes and the higher wet deposition in the spring and the summer.

Fig. 2 Frequency distribution of wind direction and GEM at wind directions at Wuzhi Mountain during monitoring period
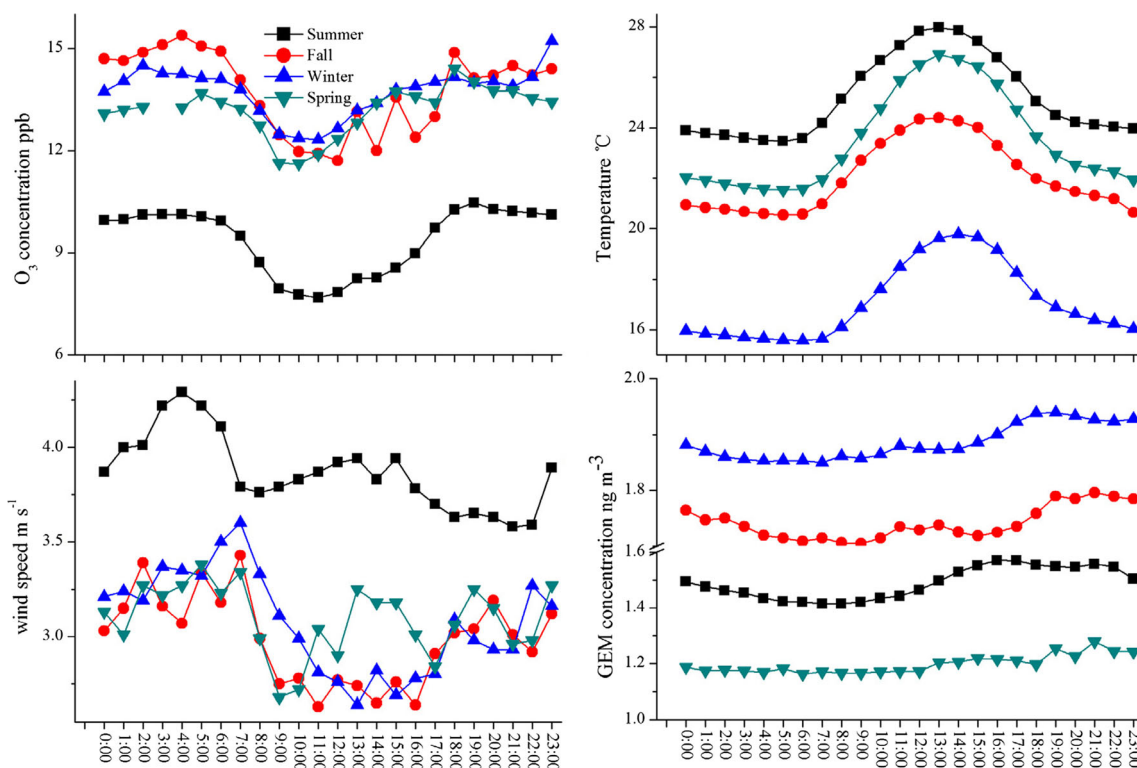
Fig. 3 Diurnal variation of GEM and ozone concentration, wind speed and temperature at Wuzhi Mountain in different seasons

GEM diurnal variation and influencing factors

GEM concentrations at the monitoring site exhibited similar diel trends in all four seasons, as well as for O_3 concentrations, and air temperatures (Fig. 3). The GEM levels changed with the wind speed, decreasing from 0:00 to 7:00 and increasing from 8:00 to 19:00 (Fig. 3). The relatively high wind speed contributes to the dispersion of pollutants, as indicated by the minimum and maximum values occurring at 7:00 and 19:00 (16:00 in summer), respectively. This diel trend with a single peak at night differs from the patterns reported at other background sites. For example, at Waliguan, there are two peaks at 8:00 during the day and 22:00 at night (Fu et al., 2012a); the peak for the Lulin and Leigong mountain sites is at approximately 15:00 (Fu et al., 2010a; Sheu et al., 2010), and the peak at the Gongga and Changbai Mountain sites is at approximately 12:00 (Fu et al., 2008, 2012b).

With respect to the diel variation, no statistically significant differences between daytime and nighttime were observed using independent-sample T Test ($p = 0.119$). This trend is
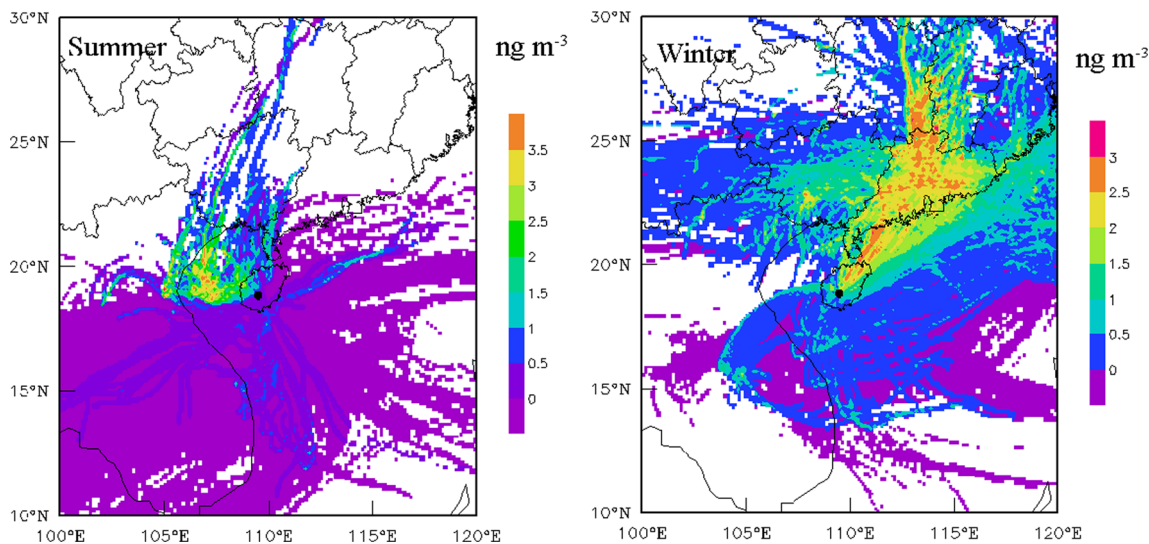
Fig. 4 CWT plots for GEM in summer and winter at Wuzhi Mountain

different from the trends reported in other studies at background sites in China (Fu et al., 2008, 2009, 2012b). These studies observed that the GEM diel trends were influenced by the mountain and valley breezes, which can cause relatively higher levels of GEM during the daytime due to the increased impact of the local and regional sources via upslope transport. However, this cannot explain the diel variation observed at Mt. Wuzhi. The elevation of the sampling site is about 1000 m a.s.l, whereas, the boundary layer height of Mt. Wuzhi were 900 m in the day and 400 m at night (Zhang et al., 2013), and the site is in the free troposphere (FT) and above the boundary layer (BL). Therefore, the air pollutants are not able to accumulate at the vertical level of this monitoring site. Additionally, contrary to the common belief, the higher O_3 concentrations actually occurred at midnight (Fig. 3), indicating that photochemical transformation did not cause the increase. The lack of local Hg sources near the site, the observed GEM and O_3 peak before midnight probably indicate the strong impact of long-range transport at the sampling site (Fu et al., 2012a).

The effects of air masses moving from different directions

The CWTs for GEM were calculated for the summer and the winter for Mt. Wuzhi (Fig. 4). The plots highlight the contributions of different source regions to the GEM at the monitoring site. In summer, the potential source regions of the GEM were the Beibu Gulf and northern Vietnam, while Hunan and Guangdong provinces were the predominant source regions in the winter, during which relatively high Hg concentrations were reported (Chen et al., 2013).

Table 1 Wind direction and air mass sources during the polluted episodes

Event	Pollution dates	Duration (h)	Hourly conc. (Min/Max) (ng m^{-3})	Prevailing wind direction	Air mass sources
1	2011.05.16–05.20	89	2.02/4.52	SW	Southwest of SCS[a], Indochina peninsula, Chinese Mainland
2	2011.05.23–06.03	268	2.24/5.82	NE	Southwest of SCS[a], Indochina peninsula, Chinese Mainland
3	2011.08.28–09.02	78	2.28/6.74	SW	Northern Vietnam, Chinese Mainland
4	2011.09.02–09.03	15	2.00/2.24	SW	Indochina peninsula
5	2011.09.05–09.06	27	2.07/2.49	SE	Indochina peninsula
6	2011.09.20–09.26	132	2.02/4.72	NE	Chinese Mainland, Taiwan
7	2011.09.26–09.27	15	2.07/2.37	NE, SE	Taiwan
8	2011.09.28–09.30	26	2.21/4.30	SW	Indochina peninsula, Chinese Mainland
9	2011.10.03–10.06	75	2.10/2.56	NE	Chinese Mainland, Taiwan
10	2011.10.16–10.19	78	2.02/2.86	NE	Chinese Mainland, China's southeast coast
11	2011.10.29–10.30	14	2.00/2.52	NE	Chinese Mainland
12	2011.11.09–11.11	26	2.13/3.31	NE	Chinese Mainland
13	2011.11.11–11.12	16	2.01/2.19	NE	Chinese Mainland
14	2011.11.14–11.15	17	2.01/2.34	NE	Chinese Mainland, China's southeast coast
15	2011.11.15–11.16	23	2.02/2.97	NE	China's southeast coast, Southern Taiwan
16	2011.11.17–11.18	17	2.01/2.39	NE	China's southeast coast
17	2011.11.19–11.21	32	2.08/3.52	NE	Chinese Mainland
18	2011.11.23–11.25	54	2.01/2.76	NE	Chinese Mainland, China's southeast coast
19	2011.12.01–12.04	64	2.07/3.35	NE	Chinese Mainland, China's southeast coast
20	2011.12.08–12.18	231	2.09/3.88	NE	Chinese Mainland
21	2011.12.18–12.19	30	2.01/2.85	NE	Chinese Mainland
22	2011.12.22–12.26	109	2.01/4.03	NE	Chinese Mainland, Taiwan, Northern Vietnam
23	2011.12.31–1.1	35	2.02/2.86	NE	Chinese Mainland
24	2012.1.04–1.05	39	2.04/3.87	NE	Chinese Mainland
25	2012.1.06–1.08	47	2.01/2.66	NE	Chinese Mainland, China's southeast coast
26	2015.1.09–1.13	109	2.03/2.91	NE	Chinese Mainland
27	2015.1.22–1.23	25	2.01/2.82	NE, SW	Chinese Mainland, China's southeast coast
28	2012.2.16–2.18	40	2.12/3.89	NE	Chinese Mainland, China's southeast coast
29	2012.3.10–3.12	69	2.01/3.83	NE	Chinese Mainland
30	2012.3.23–3.25	53	2.01/4.63	NE	Chinese Mainland, Indochina peninsula

[a] SCS means South China Sea

The pollution events were defined as hourly mean GEM concentrations higher than 2 ng m^{-3} over a period of 10 h (annual average GEM concentration plus 1/2 SD (rounded)). We observed 30 pollution episodes over the study period (Table 1). To determine the reason and the source of this high number of events, the Hybrid Single-Particle Lagrangian Integrated Trajectory model was used to calculate the backward trajectories. The results indicated that the polluted air masses mainly came from the Chinese mainland, China's southeast coast, the Indochina peninsula, and Taiwan (Table 1). For the 25 pollution episodes that are related to air masses from mainland China, Guangdong and Guangxi Provinces accounted for approximately 80 %, followed by Hunan (8 %), Jiangxi, Fujian, and Hubei Provinces. The Chinese southeast coastal regions and Taiwan also contributed to the increased GEM levels (episode 16 and episode 7, Fig. 5). In most cases, the air mass sources were of multiple origins, e.g., in Episode 2 (Fig. 5), the air mass mainly originated from three regions: Chinese mainland, China's southeast coast, and the Indochina peninsula. It is worth noting that in two instances of the 30 episodes, the pollution came entirely from the Indochina peninsula (Episodes 4 and 5, Fig. 5), particularly from northern Vietnam (Episode 3 and 22, Table 1). Overall, the long-range transport of Hg from the Chinese mainland remains the main cause of the increased GEM concentrations at the monitoring site, but we should not exclude the possibility of the long-range transport of Hg from Southeast Asia, especially in the spring. Predictably, the rapid economic development of the countries in Southeast Asia will play an increasingly important role in increasing the atmospheric Hg in the SCS, Hainan Island, and even the Chinese mainland.

Primary emission sources of GEM

CO is commonly considered to be an important tracer of anthropogenic pollution. The correlation between GEM and CO can therefore be used to identify Hg sources. Both biomass burning and anthropogenic emissions (mainly fossil fuel burning) are significant sources of CO emission (Weiss-Penzias et al., 2007). Good GEM/CO correlations were observed at Hedo Station, Okinawa (HSO) (Jaffe et al., 2005), Mount Bachelor Observatory (MBO) (Weiss-Penzias et al., 2006), and Lulin Atmospheric Background Station (ABLS) (Sheu et al., 2010). In this study, significant GEM/CO correlations were observed in autumn ($r^2 = 0.351$, $p < 0.001$), winter ($r^2 = 0.751$, $p < 0.001$), and spring ($r^2 = 0.745$, $p < 0.001$), whereas, no significant correlations were observed in summer ($r^2 = 0.064$, $p < 0.05$), consistent with the results of another study (Sheu et al., 2010). Previous studies have reported that the export of atmospheric Hg from the East Asian continent to the northern SCS by northeast monsoon activity in autumn, winter, and spring (Tseng et al., 2012; Sheu et al., 2013) can explain the significant GEM/CO correlations observed in winter and autumn. However, in this study, this explanation was seen to be invalid for spring. Clean marine air masses may account for the poor GEM/CO correlations in summer. Significant GEM/CO

Fig. 5 Daily backward trajectories ended at Wuzhi Mountain at a height of 958 m above Sea level in typical periods
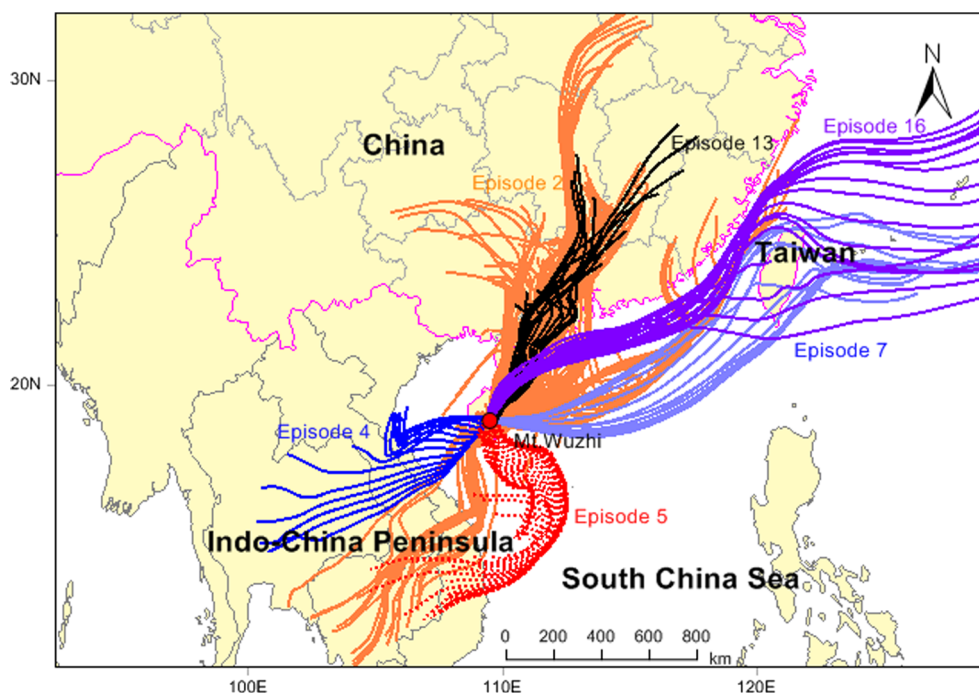
Table 2 Correlation coefficients and slopes between GEM and CO

Event	Pollution dates	GEM/CO (slope, ng m^{-3} ppbv^{-1})	GEM conc. (ng m^{-3})	CO conc. (ppbv)	r^2
2	20110524	0.0037	4.01 ± 0.48	680 ± 112	0.51
2	20110527	0.0075	4.16 ± 0.63	584 ± 66.4	0.66
6	20110922	0.0059	3.17 ± 0.48	520 ± 64	0.61
8	20110928	0.0077	2.90 ± 0.70	456 ± 80	0.80
10	20111016	0.0045	2.34 ± 0.20	470 ± 42	0.88
17	20111120	0.0022	3.00 ± 0.37	608 ± 104	0.35
20	20111209	0.0034	3.36 ± 0.33	760 ± 88	0.82
20	20111215	0.0079	2.98 ± 0.54	544 ± 60	0.76
22	20111223	0.0055	3.07 ± 0.52	592 ± 88	0.88
24	20120104	0.0037	2.76 ± 0.63	608 ± 160	0.93
28	20120216	0.0040	2.98 ± 0.48	681 ± 106	0.76
29	20120310	0.0039	2.72 ± 0.50	670 ± 110	0.80
30	20120323	0.0089	2.74 ± 0.76	498 ± 70	0.72

correlations in spring could be related to the biomass burning in the Indochina Peninsula. Spring is the major biomass burning season in the Indochina Peninsula (Streets et al., 2003; Lai et al., 2010), likely resulting in the release of Hg to the atmosphere (Friedli et al., 2009). In spring, the air masses came from the northeastern Indian Ocean and then pass over the Indochina Peninsula that can reach Mt. Wuzhi via the Southwest wind. Overall, good GEM-CO correlations in the three seasons suggest that CO and GEM share emission sources (biomass burning and anthropogenic emissions).

The △GEM/△CO enhancement ratio has been used to investigate the long-range transport of Hg (Jaffe et al., 2005; Kim et al., 2009; Fu et al., 2015). Some studies have reported an effect on long-range Hg transport from Asia when the △GEM/△CO ratio is in the range of 0.0036 ~ 0.0074 ng m^{-3} ppbv^{-1} (Jaffe et al., 2005; Weiss-Penzias et al., 2006). The GEM/CO correlation slopes for mainland China, South Asia, and the Indochina Peninsula were 0.0073, 0.0078 and 0.0078 ng·m^{-3} ppbv^{-1}, respectively (Fu et al., 2015). An episode was defined as a period with average hourly GEM and CO concentrations over 2 ng m^{-3} and 400 ppbv, respectively, for at least 10 h; 13 such episodes with simultaneously high GEM and CO concentrations and significantly positive correlations (r^2 = 0.35 ~ 0.93) are identified over the entire sampling period (Table 2). The mean GEM/CO values for East Asian industrial and biomass burning are 0.0046 ± 0.0013 ng m^{-3} ppbv^{-1} and 0.0013 ± 0.008 ng m^{-3} ppb v^{-1}, respectively (Weiss-Penzias et al., 2007). It is inferred that Episode 17 (Table 2) is predominantly caused by biomass burning. Episodes 2, 8, 20, and 30 (Table 2) seem to be of

predominantly anthropogenic origin and that many of the other episodes are of mixed origin. The mean △GEM/△CO slope for these episodes is 0.0053 ng m^{-3} ppbv^{-1} (r^2 = 0.73, $p < 0.001$), which is also consistent with the slopes reported in previous studies (Jaffe et al., 2005; Weiss-Penzias et al., 2006), indicative of the significant effect of long-range transport of Hg from China and the Indochina Peninsula.

Conclusions

The unique geographical location and a lack of local industrial Hg emissions make Hainan an ideal region to monitor the long-range transport of atmospheric Hg and other pollutants from mainland China and Southeast Asia to the SCS. At the monitoring site, the diel variation of the GEM was controlled by the wind speed and long-range atmospheric mercury transport. However, the seasonal variation of the GEM was controlled by the seasonal monsoons. The large quantity of Hg emitted from anthropogenic sources in China results in Hg being transported from the Chinese Mainland to the SCS and Hainan Island during the prevailing winter monsoon patterns. Thus, it is essential to develop more studies on the long-distance transportation capacity of Hg and the corresponding cyclical processes and ecological impacts. In addition, we noted that relatively high levels of GEM were sometimes transferred from the Southeast Asia region by air masses. With the rapid economic development of Southeast Asia, it is expected that during the seasonal monsoons, the atmospheric pollutants from this region will have stronger effects on the SCS, Hainan Island, and even the Chinese mainland in the spring and summer.

References

Chen LG, Liu M, Xu ZC, Fan RF, Tao J, Chen DH, Zhang DQ, Xie DH, Sun JR (2013) Variation trends and influencing factors of total gaseous mercury in the Pearl River Delta: a highly industrialised region in South China influenced by seasonal monsoons. Atmos Environ 77:757–766

Dou HY, Wang SX, Wang L, Zhang L, Hao JM (2013) Characteristics of total gaseous mercury concentrations at a rural site of Yangze Delta, China. Environ Sci 34:1–7 in Chinese

Fang FM, Wang QC, Li JF (2004) Urban environmental Hg in Changchun, a metropolitan city in northeastern China: source, cycle, and fate. Sci Total Environ 330:159–170

Feng XB, Shang LH, Wang SF, Tang SL, Zheng W (2004) Temporal variation of total gaseous mercury in the air of Guiyang, China. J Geophy Res 109:D03303. doi:10.1029/2003JD00419

Friedli HR, Arellano AF, Cinnirella S, Pirrone N (2009) Initial estimates of mercury emissions to the atmosphere from global biomass burning. Environ Sci Technol 43:3507–3513

Friedli HR, Arellano AF, Geng F, Cai C, Pan L (2011) Measurements of atmospheric mercury in Shanghai during September 2009. Atmos Chem Phys 11:3781–3788

Fu XW, Feng XB, Zhu WZ, Wang SF, Liu JL (2008) Total gaseous mercury concentrations in ambient air in the eastern slope of Mt.Gongga, south-eastern fringe of the Tibetan plateau, China. Atmos Environ 42:970–979

Fu XW, Feng XB, Wang SF, Rothenberg S, Shang LH, Li ZG, Qiu GL (2009) Temporal and spatial distributions of total gaseous mercury concentrations in ambient air in a mountainous area in southwestern China: implications for industrial and domestic mercury emissions in remote areas in China. Sci Total Environ 407:2306–2314

Fu XW, Feng XB, Dong ZQ, Yin RS, Wang JX, Yang ZR, Zhang H (2010a) Atmospheric gaseous elemental mercury (GEM) concentrations and mercury depositions at a high-altitude mountain peak in South China. Atmos Chem Phys 10:2425–2437

Fu XW, Feng XB, Zhang G, Xu WH, Li XD, Yao H, Liang P, Li J, Sommar J, Yin RS, Liu N (2010b) Mercury in the marine boundary layer and seawater of the South China Sea: concentrations, sea/air flux, and implication for land outflow. J Geophy Res 115:D06303. doi:10.1029/2009JD012958

Fu XW, Feng XB, Liang P, Deliger ZH, Ji J, Liu P (2012a) Temporal trend and sources of speciated atmospheric mercury at Waliguan GAW station, North-Western China. Atmos Chem Phys 12:1951–1964

Fu XW, Feng XB, Shang LH, Wang SF, Zhang H (2012b) Two years of measurements of atmospheric total gaseous mercury (TGM) at a remote site in Mt.Changbai area, northeastern China. Atmos Chem Phys 12:4215–4226

Fu XW, Zhang H, Lin CJ, Feng XB, Zhou LX, Fang SX (2015) Correlation slopes of GEM/CO, GEM/CO$_2$, and GEM/CH$_4$ and estimated mercury emissions in China, South Asia, the Indochinese peninsula, and Central Asia derived from observations in northwestern and southwestern China. Atmos Chem Phys 15:1013–1028

Gustin MS, Amos HM, Huang J, Miller MB, Heidecorn K (2015) Measuring and modeling mercury in the atmosphere: a critical review. Atmos Chem Phys 15:5697–5713

Hsu YK, Holsen TM, Hopke PK (2003) Comparison of hybrid receptor models to locate PCB sources in Chicago. Atmos Environ 37:545–562

Jaffe D, Prestbo E, Swartzendruber P, Peter WP, Kato S, Takami A, Hatakeyama S, Kajii Y (2005) Export of atmospheric mercury from Asia. Atmos Environ 39:3029–3038

Kabashnikov VP, Chaikovsky AP, Kucsera TL, Metelskaya NS (2011) Estimated accuracy of three common trajectory statistical methods. Atmos Environ 45:5425–5430

Kim KH, Ebinghaus R, Schroeder WH, Blanchard P, Kock HH, Steffen A, Froude FA, Kim MY, Hong SM, Kim JH (2005) Atmospheric mercury concentrations from several observatory sites in the northern hemisphere. J Atmos Chem 50:1–24

Kim SH, Han YJ, Holsen TM, Yi SM (2009) Characteristics of atmospheric speciated mercury concentrations (TGM, Hg(II) and Hg(p) in Seoul, Korea. Atmos Environ 43:3267–3274

Lai SC, Baker AK, Schuck TJ, van Velthoven P, Oram DE, Zahn A, Hermann M, Weigelt A, Slemr F, Brenninkmeijer CAM, Ziereis H (2010) Pollution events observed during CARIBIC flights in the upper troposphere between South China and the Philippines. Atmos Chem Phys 10:1649–1660

Ministry of Environmental Protection (MEP), China (2014) Daily air quality of all cities in China. http://datacenter.mep.gov.cn/

Muntean M, Maenhout GJ, Song SJ, Selin NE, Olivier Jos GJ, Guizzardi D, Maas R, Dentener F (2014) Trend analysis from 1970 to 2008 and model evaluation of EDGARv4 global gridded anthropogenic mercury emissions. Sci Total Environ 494-495:337–350

Sheu GR, Lin NH, Wang JL, Lee CT, Ou Yang CF, Wang SH (2010) Temporal distribution and potential sources of atmospheric mercury measured at a high-elevation background station in Taiwan. Atmos Environ 44:2393–2400

Sheu GR, Lin NH, Lee CT, Wang JL, Chuang MT, Wang SH, Chi KH, Ou Yang CF (2013) Distribution of atmospheric mercury in northern Southeast Asia and South China Sea during Dongsha experiment. Atmos Environ 78:174–183

Slemr F, Brunje EG, Ebinghaus R, Temme C, Munthe J, Wängberg I, Schroeder W, Steffen A, Berg T (2003) Worldwide trend of atmospheric mercury since 1977. Geophys Res Lett 30:1516. doi:10.1029/2003GL016954

Slemr F, Angot H, Dommergue A, Magand O, Barret M, Weigelt A, Ebinghaus R, Brunke EG, Pfaffhuber KA, Edwards G, Howard D, Powell J, Keywood M, Wang F (2015) Comparison of mercury concentrations measured at several sites in the southern hemisphere. Atmos Chem Phys 15:3125–3133

Streets DG, Yarber KF, Woo JH, Carmichael GR (2003) Biomass burning in Asia: annual and seasonal estimates and atmospheric emissions. Glob Biogeochem Cycles 17:1099. doi:10.1029/2003GB002040

Su J, Cheng JP, Ye XF, Yuan T, Wang WH, Mi LJ (2007) Preliminary study on mercury distribution in multimedia environment in Lanzhou. J Agro-Environ Sci 26:381–355 in Chinese

Tseng CM, Liu CS, Lamborg C (2012) Seasonal changes in gaseous elemental mercury in relation to monsoon cycling over the northern South China Sea. Atmos Chem Phys 12:7341–7350

UNEP (2013) Global mercury assessment 2013 (2013) sources, emissions, releases and environmental transport. UNEP Chemicals Branch, Geneva

Wang YQ, Zhang XY, Draxler R (2009) TrajStat: GIS-based software that uses various trajectory statistical analysis methods to identify potential sources from long-term air pollution measurement data. Environ Model & Soft 24:938–939

Weiss-Penzias P, Jaffe D, Swartzendruber P, Dennison JB, Chand D, Hafner W, Prestbo E (2006) Observations of Asian air

pollution in the free troposphere at Mount Bachelor Observatory during the spring of 2004. J Geophys Res 111: D10304. doi:10.1029/2005JD006522

Weiss-Penzias P, Jaffe D, Swartzendruber P, Hafner W, Chand D, Prestbo E (2007) Quantifying Asian and biomass burning sources of mercury using the Hg/CO ratio in pollution plumes observed at the Mount Bachelor Observatory. Atmos Environ 41:4366–4379

Zhang L, Wang S, Wang L, Wu Y, Duan L, Wu Q, Wang F, Yang M, Yang H, Hao J, Liu X (2015) Updated emission inventories for speciated atmospheric Hg from anthropogenic sources in China. Environ Sci Technol 49:3185–3194

Zhang ZZ, Cai XH, Song Y, Kang L, Huang X, Li Q (2013) Temporal and spatial variation of atmospheric boundary layer height over Hainan Island and its adjacent sea areas. Acta sci nat univ pekinensis 49:783–790 in Chinese

Zhu J, Wang T, Talbot R, Mao H, Hall CB, Yang X, Fu C, Zhuang B, Li S, Han Y, Huang X (2012) Characteristics of atmospheric total gaseous mercury (TGM) observed in urban Nanjing, China. Atmos Chem Phys 12: 12103–12118